

X-Ray Microanalysis Investigation of the Changes in Na, K, and Hemoglobin Concentration in *Plasmodium falciparum*-Infected Red Blood Cells

Jakob M. A. Mauritz,^{†‡} Rachel Seear,[‡] Alessandro Esposito,^{†‡} Clemens F. Kaminski,^{†§} Jeremy N. Skepper,[‡] Alice Warley,[¶] Virgilio L. Lew,[‡] and Teresa Tiffert^{‡*}

[†]Department of Chemical Engineering and Biotechnology and [‡]Department of Physiology, Development and Neuroscience, University of Cambridge, Cambridge, United Kingdom; [§]School for Advanced Optical Technologies, Friedrich-Alexander-Universität Erlangen-Nürnberg, Erlangen, Germany; and [¶]Centre for Ultrastructural Imaging, King's College London, London, United Kingdom

ABSTRACT *Plasmodium falciparum* is responsible for severe malaria. During the ~48 h duration of its asexual reproduction cycle in human red blood cells, the parasite causes profound alterations in the homeostasis of the host red cell, with reversal of the normal Na and K gradients across the host cell membrane, and a drastic fall in hemoglobin content. A question critical to our understanding of how the host cell retains its integrity for the duration of the cycle had been previously addressed by modeling the homeostasis of infected cells. The model predicted a critical contribution of excess hemoglobin consumption to cell integrity (the colloid osmotic hypothesis). Here we tested this prediction with the use of electron-probe x-ray microanalysis to measure the stage-related changes in Na, K, and Fe contents in single infected red cells and in uninfected controls. The results document a decrease in Fe signal with increased Na/K ratio. Interpreted in terms of concentrations, the results point to a sustained fall in host cell hemoglobin concentration with parasite maturation, supporting a colloid osmotic role of excess hemoglobin digestion. The results also provide, for the first time to our knowledge, comprehensive maps of the elemental distributions of Na, K, and Fe in *falciparum*-infected red blood cells.

INTRODUCTION

The intraerythrocytic stage of the *Plasmodium falciparum* cycle is responsible for the symptoms of malaria. Invasion of red blood cells (RBCs) by *falciparum* merozoites alters the host cell metabolism, composition, membrane transport, osmotic fragility, and rheological properties, with a well-characterized progression (1). After an initial quiescent period of ~15–20 h postinvasion, glycolytic metabolism increases by two orders of magnitude (2,3) and new permeation pathways (NPPs) become activated in the host-cell membrane to allow for an increased traffic of nutrients and waste products (1,4–9). NPPs mediate a rapid dissipation of the normal RBC Na and K gradients, thus surrounding the developing parasite with a high-Na, low-K extracellular environment within the host cell (10–14). This is of functional significance for Na-energized cotransport across the parasite plasma membrane (15). However, the increased cation permeability also poses a serious threat of rapid cell swelling and premature host cell lysis by the unbalanced gain of NaCl and water (12). After NPP development, there is a sharp increase in hemoglobin (Hb) ingestion and digestion by the parasite which progresses to an excess far beyond the protein synthetic needs of the parasite (16). Greater than 70% of the host-cell Hb is ultimately

consumed, and greater than 80% of the amino acids generated from Hb digestion are released as waste through the NPPs (17).

A major challenge posed by these events was to explain how the host cell maintained its integrity for the 48 h duration of the asexual reproduction cycle of the parasite (12). An analysis of the homeostasis of *falciparum*-infected RBCs (IRBCs), encoded in a mathematical-computational model of IRBC homeostasis (18,19), suggested an explanation, the colloid osmotic hypothesis, which linked the excess Hb digestion to the osmotic stability of the infected cell (18–20). According to this hypothesis, excess Hb digestion was required to reduce the colloid osmotic pressure within the host cell so that the unbalanced rate of NaCl gain through the NPPs and consequent swelling could be contained within limits that would not compromise the integrity of the osmotically fragile infected cells (18–20).

The most critical condition for the validity of the colloid osmotic hypothesis is that the concentration of Hb within the host cytosol has to fall, because the osmotic pressure exercised by Hb, π_{Hb} , is proportional to the product of its osmotic coefficient, f_{Hb} , and the Hb concentration in cell water, [Hb]: $\pi_{\text{Hb}} = RT \cdot f_{\text{Hb}} \cdot [\text{Hb}]$ (21–23), where R is the gas constant and T the absolute temperature. This condition remained controversial (22–26) and is the main focus of the investigation reported here.

We have used electron-probe x-ray microanalysis (EPXMA) to estimate [Hb] by measuring the local elemental Fe, Na, and K composition in host cytosolic domains using the Na/K ratio as a developmental stage marker. EPXMA (which is an electron microscopy (EM) technique)

Submitted December 7, 2010, and accepted for publication February 1, 2011.

*Correspondence: jtt1000@cam.ac.uk

Alessandro Esposito's present address is MRC Cancer Cell Unit, Hutchison/MRC Research Centre, Hills Road, CB20XZ, Cambridge, UK.

Editor: Paul W. Wiseman.

has the advantage for this investigation that it allows the concentrations of all elements to be measured simultaneously, and, because the area for analysis is selected from the visual image, the concentrations are localized directly to specific regions of the sectioned erythrocytes. In RBCs with ring or young trophozoite parasite stages we expected a high Fe signal associated with a low Na/K ratio, whereas in IRBCs with mature parasites we expected a lower Fe signal associated with a higher Na/K ratio. The original hemoglobin concentration in the host cytosol was estimated from the element signals by applying an algorithm which is independent of the variability in absolute concentrations that can occur with this technique. In addition, we present here for the first time (to our knowledge) comprehensive x-ray maps of the Na, K, and Fe distribution in IRBCs and a quantitative analysis of host cytosol composition in IRBCs with trophozoite stage parasites.

MATERIALS AND METHODS

Chemicals and solutions

Solution A contained NaCl, 145 mM; KCl, 3 mM; Na-HEPES (pH 7.5 at 37°C), 10 mM; and MgCl₂, 0.15 mM.

Solution AE had the same composition as solution A, but with the addition of 0.1 mM EGTA.

The solutions used for the nystatin controls were named LA, LB, WA, WB, NA, NB, and M. Their composition was:

LA: NaCl, 10 mM; KCl, 130 mM; and sucrose, 55 mM.

LB: NaCl, 130 mM; KCl, 10 mM; and sucrose, 55 mM.

WA and WB: same composition as LA and LB, respectively, with the addition of 1 mM Na-HEPES (pH 7.4 at 37°C) and 0.1% human serum albumin.

NA and NB: same composition as LA and LB, respectively, with the addition of nystatin to a final concentration of 40 μM (from a stock solution of 20 μg/μL in DMSO, equivalent to 20 mM).

M: MgCl₂, 110 mM.

All chemicals were analytical reagent quality. With the exception of the gelatin solution (Plasmagel; Bellon, Neuilly Sur Seine, France), RPMI-1640 culture medium and all other chemicals were from Sigma-Aldrich, Gillingham, Dorset, UK.

Cultures and preparation of cells

Red cells infected with *P. falciparum* clones ITO4 and A4BC6 (kindly provided by B. C. Elford, Institute of Molecular Medicine, Oxford, UK) (24), and strain POM19 (kindly provided by E. Gotuzzo, Instituto de Medicina Tropical Alexander von Humboldt, Universidad Peruana Cayetano Heredia, Lima, Peru) were cultured under a low-oxygen atmosphere by standard methods (25). The culture medium was RPMI-1640 supplemented with 40 mM HEPES, 25 mg/L gentamicin sulfate, 10 mM D-glucose, 2 mM glutamine, and 0.5% albumax II. Parasite development and replication were assessed in cultures by microscopic inspection of Giemsa-stained thin blood smears and parasite count, as reported before (26). IRBCs containing mature trophozoites were concentrated from culture samples in different developmental stages by gelatin flotation (27,28) immediately before freezing. Further synchronization was not warranted because data analysis was focused on the correlation between EM imaging and elemental Na/K ratio for assessment of parasite developmental stage in each sample.

Preparation of nystatin-treated RBCs

To ascertain the reliability of the EXPMA-based estimates of cell Na and K concentrations, the Na and K content of fresh RBCs from healthy volunteers was altered by the nystatin method (29,30) to generate high-Na and high-K RBCs covering the range of mean sodium/potassium concentration ratios expected in normal (~0.2) and trophozoite-stage infected (>5) red blood cells. RBCs were obtained from healthy volunteers by venipuncture into a syringe with heparin after informed, written consent. The RBCs were washed three times by centrifugation and resuspension in >10 volumes of solution AE, and once in solution A. The buffy coat was removed after each wash. After the last wash, the cells were distributed in three equal aliquots: one to serve as an untreated control was suspended in solution A, and of the others one was equilibrated for 20 min in high-K medium NA, and the other one in high-Na medium NB, both containing nystatin. The hematocrit was 10% and all the suspensions were kept on ice. Nystatin was removed by washing the cells four times in A, WA, or WB, respectively, with three final washes of all samples in isotonic MgCl₂ (solution M) to remove extracellular Na and K before EXPMA analysis.

Sample processing for electron microscopy

Samples containing RBCs in suspension in 1.5 mL nominal capacity microfuge tubes were briefly spun down and the supernatant removed. Wooden cocktail sticks were dipped into the cell pellet, which was then quickly plunge-frozen in liquid propane, then cooled in liquid nitrogen (−196°C), immobilizing the elements of interest (31,32). The frozen pellet was cut into thin sections of 180 nm thickness at −100°C in an ultramicrotome cryo-sectioning stage (Leica UltraCutS with fluorescence correlation spectroscopy; Leica Microsystems, Wetzlar, Germany). The sections were put on carbon film-coated nickel grids and subsequently transferred under liquid nitrogen into a turbo molecular-pumped carbon coater (Auto 306; Edwards, Crawley, UK) where they were freeze-dried overnight and carbon-coated. The EM grids were stored in a dessicator until analysis.

Electron microscopy and x-ray microanalysis

For the EXPMA analysis the samples were transferred at room temperature into a transmission electron microscope (Tecnai T12; FEI, Hillsboro, OR) fitted with an electron beam and image deflection board to allow collection of x-ray maps (33), and a Si(Li) energy dispersive x-ray detector (EDAX, Tilberg, The Netherlands). For the x-ray microanalysis, the microscope was operated at 120 kV in nanoprobe mode using a probe size of roughly 10 nm diameter. The grid was tilted 25° toward the detector. The relative detector sensitivity (*S*-values) was calibrated for Na, K, and Fe with Na-K-tartrate and K-ferricyanate in gelatin. For spectrum analysis and element mapping, EDAX Genesis software (EDAX; Tilberg, The Netherlands) was used. Data of the electron-probe-measured elemental composition were recorded from between 5 and 40 different cells in each sample, and the results are reported as the mean and standard error of the mean.

Quantifying cytosol composition

The calibrated electron-probe data obtained from freeze-dried cryosections are reported in units of mmol/(Kg dry weight), or mmol/Kg. A main aim in this investigation was to estimate the hemoglobin concentration in the red cell cytoplasm in units of mmol/(liter cell water), or mmol/L_{cw}. This required a reliable conversion procedure for both uninfected controls and infected RBCs, independent of the nature of the dry weight material. Searching for a reliable conversion strategy (34), we developed one based on the well-established fact that RBCs attain and maintain osmotic equilibrium across their plasma membrane because of their high water

permeability (35). For uninfected RBCs equilibrated in solution A (~300 mOsM) before freezing, the intracellular concentrations of Na plus K in cell water ($[Na]+[K]$) would have to be very near 150 mmol/Lcw because K and Na are the main intracellular cations available to balance the negative charges on cell anions (35).

Let cNa and cK represent the respective electron-probe-measured elemental composition of Na and K in each spot, in units of mmol/(Kg dry weight). The ratio $f = (cNa+cK)/([Na]+[K])$, in units of Lcw/Kg, renders the volume of cell water associated with a unit Kg dry weight of each imaged spot in the cryosection. We can now divide the elemental composition of Fe in that sample, cFe , by f to obtain the monomeric hemoglobin concentration in units of mmol/Lcw. Thus, the concentration of the Hb tetramer, $[Hb]$, in units of mmol/Lcw, will be given by: $[Hb] = cFe/(4f)$. Similarly, the electron-probe-measured Na and K concentrations per Kg dry weight, cNa , and cK , respectively, can be converted to the original concentrations of Na and K in RBC water, $[Na]$, and $[K]$, in units of mmol/Lcw, using $[Na] = cNa/f$ and $[K] = cK/f$. The individual electron-probe concentrations retrieved from each imaged spot differ greatly.

The cX -to- $[X]$ conversion defined above normalizes all values to comparable quantities, and, as shown in Results, renders values well within the expected ranges for uninfected RBCs and nystatin-treated controls. Because osmotic equilibrium may be assumed to prevail across plasma membranes of IRBCs and parasites, the same general approach was applied to estimate concentrations within the cytoplasm of parasites and IRBCs. For parasites, in the absence of detailed information and alternative options we tentatively assumed that $[Na]+[K] = 150$ mmol/Lcw for the estimate of f . Hence, the values obtained ought to be considered first approximations. For the cytoplasm of IRBCs, we took into account the minor stage-related variations in IRBC $[Na]+[K]$ suggested by analysis of IRBC model predictions, as reported later in Fig. 4 A.

RESULTS

Sample x-ray spectra

Fig. 1 shows representative x-ray spectra of cytosolic domains of uninfected (A) and trophozoite-stage infected (B) red blood cells, and of the parasite cytoplasm away from the food vacuole (C). In the uninfected RBC, K is the dominant peak (Fig. 1 A), whereas in the infected red cell Na is dominant and the K peak is much reduced (Fig. 1 B). In the parasite cytoplasm (Fig. 1 C), K is again dominant over Na, and shares dominance with phosphate (P), reflecting high metabolic activity and nucleotide turnover. The Fe peak is present in the cytosol of the red cells but is vanishingly small in parasite cytoplasm. The P and S elemental peaks are also shown, but were not investigated

further here. The Si signal corresponds to desiccant contamination.

Elemental x-ray maps

Representative EM images of IRBC thin sections are shown with their corresponding x-ray maps in Fig. 2. The maps represent the elemental distribution of Na, K, and Fe in a color-coded red-green-blue overlay. The algorithm used for visualization renders the colors resulting from mixing red (for K), green (for Na), and blue (for Fe) according to their relative intensities in each pixel, so that, e.g., a violet color in the map corresponds to a region high in both Fe and K and yellow corresponds to a region high in both Na and K.

Fig. 2 A shows an electron micrograph of an uninfected RBC section. Adjacent to the cell the salt contents of the (freeze-dried) cell suspension medium can be seen as transparent matrix. In the corresponding x-ray map (Fig. 2 B), the extracellular region presents a strong Na signal and is low in Fe and K. At the cell boundary, the sharp transition of the dominant element from Na to K can be clearly seen, with the cytosol high in K (red) and low in Na (green). The Fe signal (blue) is homogeneous throughout the cell.

Fig. 2 C shows an electron micrograph of an IRBC with a mature trophozoite. The host cytosol appears uniformly dark and clearly distinguishable from the brighter parasite region. In the food vacuole, the hemozoin crystals can be seen as dark spots. The corresponding x-ray map (Fig. 2 D) displays a stark contrast between parasite (high K) and host cytosol (high Na). The dominant iron signals in Fig. 2, D and F, colocalize with the iron-rich hemozoin crystal images in the corresponding micrographs (Fig. 2, C and E). Note the remarkable similarity between the green-red transitions across the medium-cell boundary in Fig. 2 B and across the host-parasite boundaries in Fig. 2, D and F, illustrating visually the extracellular-like high-Na, low-K environment surrounding the parasite within the host red cell.

Fig. 2 E depicts an electron micrograph of two IRBCs with mature trophozoites and two adjacent RBC fragments. The cells in this image, from a trophozoite-enriched sample with no ring-stage parasites, had been washed in isotonic

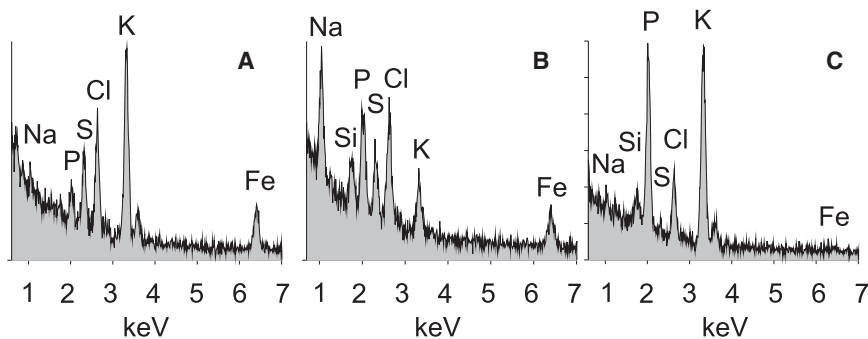


FIGURE 1 Representative x-ray spectra of uninfected RBCs, falciparum-infected RBCs, and parasite cytoplasm. The element label in each panel is directly above the respective $K_{\alpha 1}$ -transition peak. (A) Uninfected RBC, high in K and low in Na; (B) RBC host to trophozoite-stage parasite, high in Na and low in K. (C) Parasite cytoplasm, high in K and low in Na; the large P peak signals high metabolic activity. The present Ni peak of the EM grid and the C, O, and N peaks of the sample are beyond the energy range shown. The Si-peaks are an artifact stemming from the desiccant.

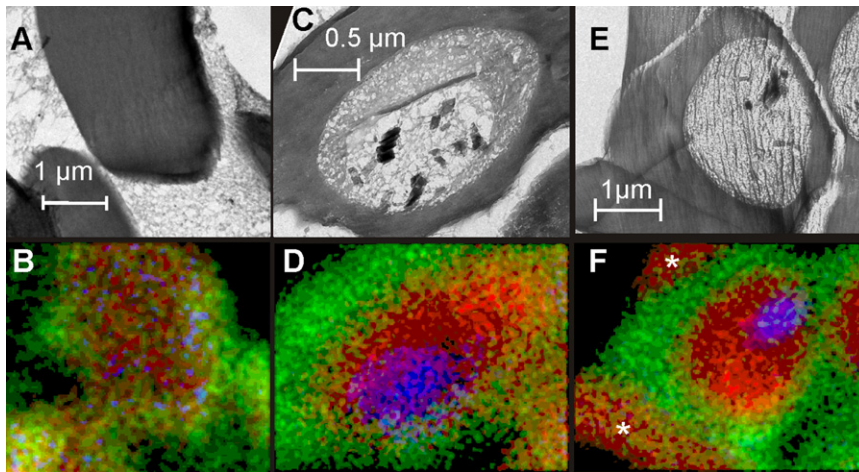


FIGURE 2 EPXMA elemental maps of the Na, K, and Fe distributions in uninfected RBCs and infected RBCs with trophozoite-stage parasite. EM images (*top row*) are shown vertically aligned with the corresponding EPXMA images (*bottom row*). Correspondence between the photographed image and the mapped field is not perfect because the transmission electron microscopy imaging camera used is not an integral part of the mapping system. The EPXMA maps are assembled as a red-green-blue overlay of the Na (*green*), K (*red*), and Fe (*blue*) x-ray raw peak count for each spot. Mixtures of these colors can result, e.g., in yellow (both high K and Na), or violet (both high Fe and K). (A and B) Uninfected RBC surrounded by salt crust from the dried extracellular medium. (C and D) IRBC with trophozoite-stage parasite and food vacuole. The black spots are hemozoin crystals responsible for the high Fe signal. (E and F) IRBC with trophozoite-stage parasite next to two uninfected RBCs (*white starred*).

MgCl₂ before freezing, thus removing x-ray signals from the extracellular medium. In the electron micrograph (Fig. 2 E) it is impossible to tell whether the adjacent cell fragments correspond to uninfected cells. But the x-ray map in Fig. 2 F reveals the high-K content of the cell fragments, indicating that they correspond to uninfected RBCs.

Sodium, potassium, and iron (hemoglobin) concentrations within host-cell and parasite domains

Fig. 3 A shows a representative sample of electron-probe-measured elemental Na, K, and Fe composition obtained from the cytoplasm of uninfected control RBCs and from uninfected cohort RBCs separated from a live *P. falciparum* culture. The results show the typical low-Na, high-K pattern of normal, uninfected RBCs. The estimated cytoplasmic concentrations of Na, K, and Hb derived from these measurements, using $[Na] = cNa/f$, $[K] = cK/f$, and $[Hb] = cFe/(4f)$ (see *Materials and Methods*), are shown in Fig. 3 B and report values well within the variation range found in RBCs from healthy human adults. The estimated mean Hb concentration in all RBC samples analyzed was 6.5 ± 0.2 mM ($n = 33$).

Nystatin (see *Materials and Methods*) was used to generate RBCs with inverted Na/K contents to test the reliability of the electron probe to accurately report such variations. The measurements obtained are shown in Fig. 3 C, and the derived concentrations in Fig. 3 D. It can be seen that the inverted Na/K ratio (Fig. 3 E) was accurately reproduced, establishing the validity of electron-probe measurements of Na/K concentration ratios within the cytoplasm of infected RBCs as an approximate indicator of parasite developmental state.

Fig. 4 A reports the analysis of the minor stage-related variations in IRBC $[Na]+[K]$ of IRBC suggested by model

predictions (18). Fig. 4 B shows a comparison between electron-probe-derived concentrations of Na, K, and Fe in the cytoplasm of host and parasite, obtained from IRBCs with mature trophozoites. Parasite cytoplasm data was acquired as far away from the food vacuole as was possible, to avoid signal contribution from the high Fe content of the hemozoin crystals. At this developmental stage, the probe detected a high-Na, low-K pattern in the host cytoplasm, and the opposite pattern within the parasite cytoplasm (Fig. 4 B, *inset*) confirming earlier measurements in host cells and parasites (10–14,36). The Hb concentration of 2.8 mmol/Lcw in the host corresponds to a reduction of >50% from mean normal levels. The origin of the Fe signal and of the Fe/4 value of 1.6 mmol/Lcw within the parasite cytosol may be attributed to endostomal Hb or heme proximity, but cannot be identified from these measurements.

The results of 155 electron-probe Na, K, and Fe measurements in the cytoplasm of IRBCs with parasites in different developmental stages are shown in Fig. 5. The hemoglobin concentration is plotted as a function of the Na/K concentration ratio, with higher ratio values suggesting more advanced developmental stages. The results expose a clear trend of decreasing hemoglobin concentration with increasing Na/K ratio, but the rate of decline with Na/K ratio shows two distinct patterns, of sharp and gentle decline, in IRBCs from different cultures.

DISCUSSION

EPXMA imaging has been used here to document the distribution of Na, K, and Fe in *P. falciparum*-infected red blood cells. The x-ray maps shown in Fig. 2 illustrate this distribution in the different subcellular domains of IRBCs. The maps confirm earlier results obtained by different methods (8–12) showing that during *P. falciparum* infection, the

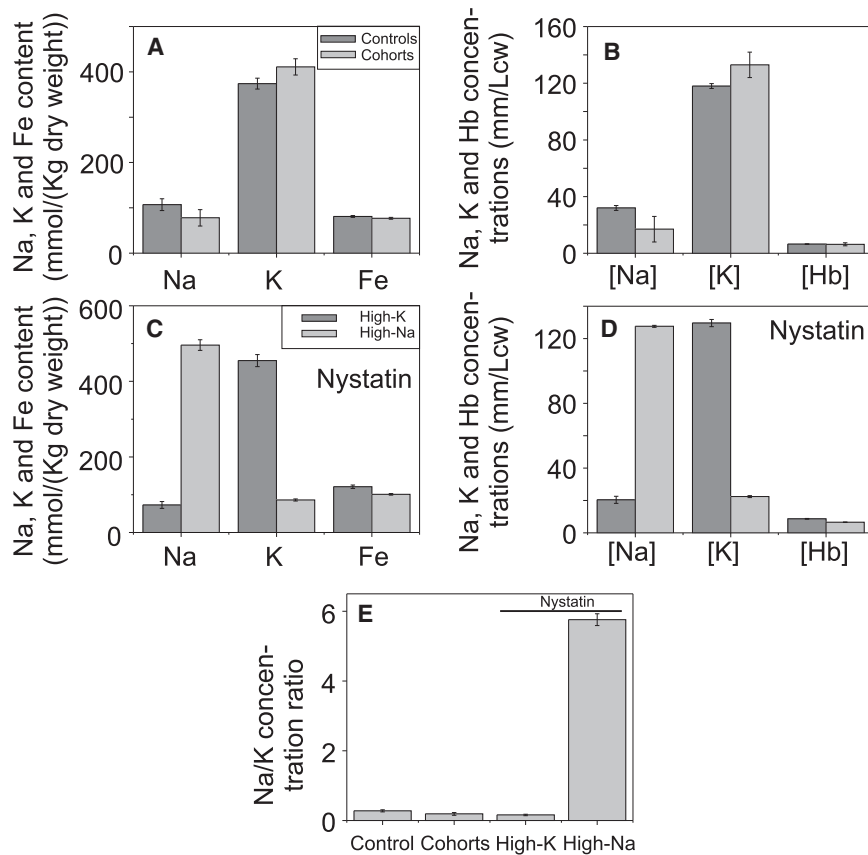


FIGURE 3 Electron-probe-measured contents and concentrations of Na, K, and Fe in uninfected RBCs. Bars and error bars represent means and standard error of the means. (A and C) Electron-probe raw readings of Na, K, and Fe. (B and D) The Na, K, and Fe signals were converted to concentrations in mmol/(liter cell water) as explained in Materials and Methods; the Fe signal was converted to tetrameric hemoglobin concentration, [Hb]. (A and B) Cytosol composition of Na, K, and Fe of control RBCs ($n = 33$) and of uninfected cohort RBCs from mature trophozoite cultures ($n = 5$). (C and D) Cytosol composition of Na, K, and Fe of nystatin-pretreated RBCs in high-K media ($n = 20$) and in high-Na media ($n = 25$). $p < 0.001$ (t -test) for the differences in Na and K contents (C) and concentrations (D) between high-K and high-Na conditions; $p < 0.01$ for the corresponding differences in Fe (C) and [Hb] (D). (E) Comparison of the Na/K concentration ratio for the four samples above. $p < 0.001$ for the difference between the ratio in the high-Na nystatin condition and the other three conditions.

cation composition of the host cell cytoplasm changes dramatically, with dissipation of the normal Na/K gradients across the RBC membrane, whereas the parasite cytoplasm retains a typical high-K, low-Na intracellular environment. The maps also show the distribution of iron-containing molecules, hemoglobin and hemozoin.

The more quantitative estimates derived from the electron-probe measurements of Na, K, and Fe (Figs. 4 and 5) confirm the overall qualitative description provided by the x-ray maps, and provide independent evidence of a decline in hemoglobin concentration associated with elevated Na/K concentration ratios within the host cell cytoplasm. These results then confirm previous observations of stage-related decline in Hb concentration obtained with different optical methods (37,38) and add support to the view that excess Hb consumption contributes to retain the integrity of the osmotically fragile IRBCs (18,19,39) by reducing the colloid osmotic pressure within the host cell. The colloid osmotic hypothesis was recently challenged in experiments with protease inhibitors (40). According to the hypothesis, prevention of Hb digestion with the use of protease inhibitors should lead to premature IRBC lysis. In early (20) and recent attempts (40), no premature lysis was detected. However, in both attempts, it proved impossible to block Hb consumption without impairing parasite development at the same time. In these conditions, failure to detect

increased lysis or osmotic fragility has no relevance as a test of the colloid osmotic hypothesis because the IRBCs never reach the stage of osmotic compromise.

The two apparent patterns of decline in Hb concentration with Na/K ratio shown in Fig. 5 may represent accidental differences without particular significance beyond occasional experimental variations, or they may reflect a real duality deserving further consideration. We applied the mathematical-computational model of IRBC homeostasis (18–20), which encodes our current understanding of the homeostasis of *P. falciparum*-infected RBCs, to search for clues about possible biological variations that may explain the steep and gentle [Hb] decline patterns observed. The search was on for the minimal set of parameter values that could provide adequate fits of the experimental points in Fig. 5.

The approximate fits for both [Hb] decline modalities shown in Fig. 6 A were obtained by varying a single critical parameter, the ratio of the membrane permeabilities to K^+ and Na^+ (PK/PNa ratio), representing the Na-K selectivity attributed to NPPs. Additional fine-tuning was possible by minor adjustments in other parameters, but PK/PNa remained the only critical parameter, irreplaceable for the fit. Mean values of PK/PNa of 2.3 reported by Staines et al. (12) rendered a decline curve that approximated well the gentle decline pattern. To fit the sharp decline pattern

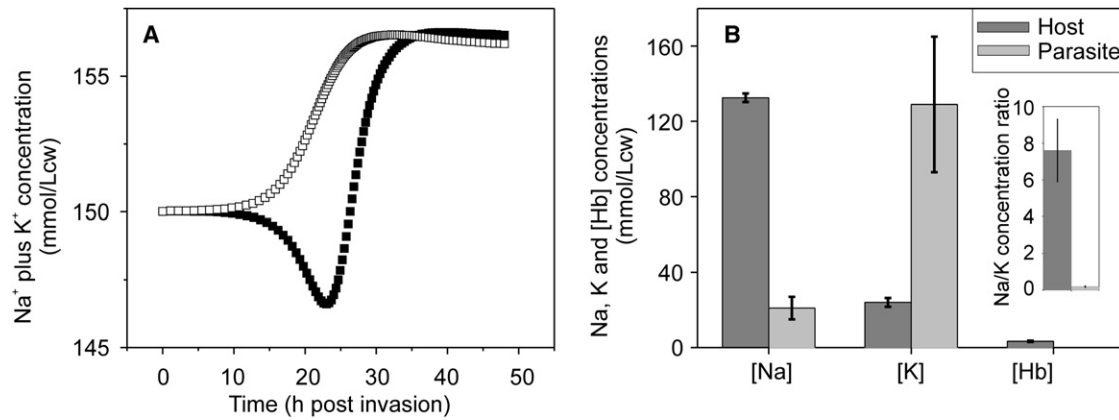


FIGURE 4 (A) Predicted stage-related changes in IRBC [Na]⁺[K]⁺ concentrations. (B) Electron-probe-based estimates of Na and K concentrations in the cytoplasm of host RBCs and parasites, obtained from IRBCs with mature parasites, and Hb concentrations estimates in cytoplasm of host RBCs (same IRBCs as for Na and K concentrations). (Inset of B) Na/K concentration ratio in host RBCs and parasites. (A) Stage-related changes in the [Na]⁺[K]⁺ concentration of IRBCs predicted by the IRBC model for different PK/PNa selectivities through NPPs: 2.3 (solid symbols) and ~1 (open symbols). With these patterns, the value of f was estimated with [Na]⁺[K]⁺ = 150 mmol/Lcw for IRBCs with ring-stage parasites, and with [Na]⁺[K]⁺ = 156 mmol/Lcw for IRBCs with trophozoite-stage parasites and activated NPPs, as estimated from elevated Na/K concentration ratios. (B) Bars represent mean and standard error of the mean of 15 host cells and 14 parasites. The Fe signal from the red cell cytosol was converted to tetrameric Hb concentration [Hb] as explained in Materials and Methods. The Fe signal from parasite cytosol was ignored for this graph. (Inset) Na/K concentration ratio, confirming the marked difference in Na-K composition between host and parasite cytoplasm at the trophozoite developmental stage. $p < 0.001$ for the differences in [Na], [K], and Na/K ratio between host and parasite. The algorithm used for these simulations is described in Mauritz et al. (18). Using the nomenclature from that article, the other model parameters were: $CF = 0.3$, $Hb_{max} = 0.7$, $t_{Hb} = 32$ h, $t_{Hb} = 27$ h, and $s_{NPP} = s_{Hb} = 3$ h⁻¹.

it was necessary to abolish the cation selectivity of the NPP pathway with PK/PNa values near 1 (Fig. 6 A). To understand how this relatively minor parameter adjustment in the residual cation selectivity of a major anion-selective pathway (1) can produce such a marked difference in the pattern of [Hb] decline, it is necessary to analyze the asso-

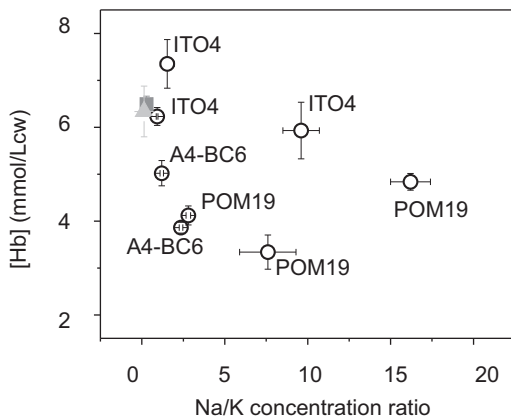


FIGURE 5 Correlation between changes in hemoglobin concentration and Na/K concentration ratio in the cytoplasm of IRBCs with trophozoite stage parasites. Increases in Na/K ratio caused by progressive dissipation of Na-K gradients through the NPP-permeability pathway are assumed to reflect advancing stages in the asexual reproduction cycle of the parasite within its host red cell. The results report electron-probe-based measurements of [Hb] in 155 IRBCs from eight different cultures. The strains used for each point are shown on the figure. (Points and cross-hairs) Mean and standard error of the mean of independent measurements obtained from between 15 and 25 cells in each sample. (Open circles) IRBCs; (square) uninfected controls ($n = 33$); and (triangle) uninfected cohort RBCs ($n = 5$).

ciated time-dependent changes in [Na], [K], and [Hb], the relevant model variables in the plot of Fig. 5.

Fig. 6, B and C, shows the patterns of Na-K gradient dissipation and of tetrameric [Hb] decline as a function of time postinvasion predicted by model simulations with (solid symbols) and without (open symbols) PK/PNa selectivity. It can be seen that whereas the [Na], [K], and [Na]/[K] ratio changes are almost identical in both conditions, the time-course and pattern of the [Hb] changes are markedly different. As the extent and timing of Hb consumption was set identical for both conditions in the modeled simulations, any changes in [Hb] could only result from host-cell water-volume variations induced by the different NPP selectivities. The predicted time-course of host-cell water-volume changes is shown in Fig. 6 D. The mechanisms responsible for these changes when PK/PNa is set to 2.3 (12) have been reported and analyzed before (18,41). Briefly, with $PK > PNa$, the onset of NPP permeabilization causes transient dehydration because initially K^+ loss exceeds Na^+ gain for a brief period of time. As the K^+ -gradient dissipates, Na^+ influx soon exceeds K^+ efflux causing delayed but sustained osmotic water gain. Without cation selectivity, on the other hand, the initial dehydration is absent (Fig. 6 D) because Na^+ gain exceeds K^+ loss all along. The ensuing sustained swelling from the start of NPP permeabilization (Fig. 6 D), which lasts for most of the intense Hb consumption period, causes a fall in Hb concentration much earlier than when $PK > PNa$ (Fig. 6 C). The initial [Hb] peak, responsible for the biphasic pattern predicted for the condition with $PK > PNa$, is thus absent when selectivity is removed (Fig. 6, A and C).

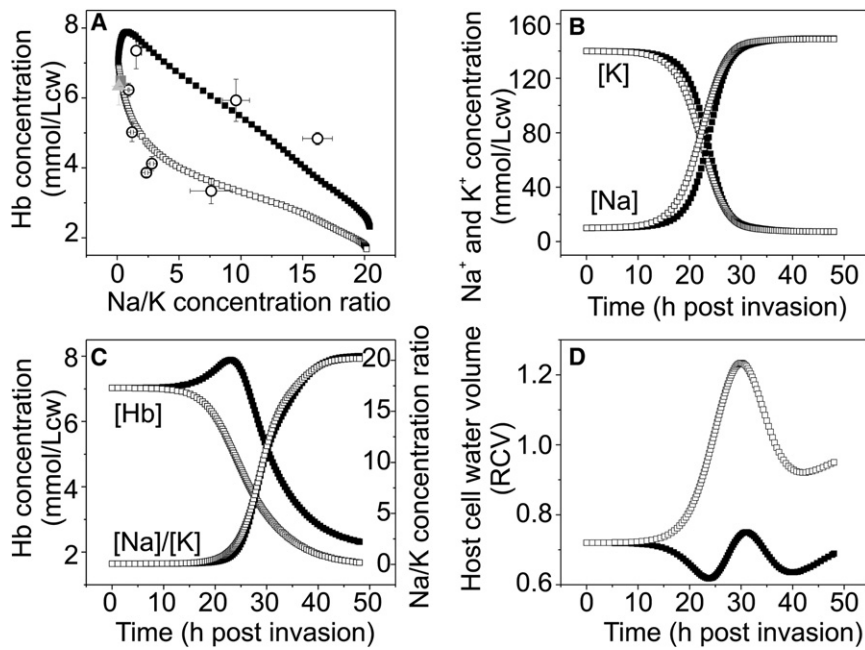


FIGURE 6 Model analysis of the electron-probe-measured [Hb]-decline patterns. The model of IRBC homeostasis (18,19) was used to search for the parameter variations required to provide approximate fits to the measured steep and gentle [Hb]-decline patterns reproduced here in the experimental points (A). A single parameter change, P_K/P_{Na} , the Na-K selectivity of the NPP permeability pathway, proved necessary and sufficient to provide the fits depicted here in panel A for the curves outlined by solid ($P_K/P_{Na} = 2.3$) and open ($P_K/P_{Na} = 0.9$) square symbols, corresponding to the gentle and steep [Hb]-decline patterns, respectively. All other parameters were the same for both simulations. Using the nomenclature in Mauritz et al. (18): $CF = 0.3$, $Hb_{max} = 0.7$, $t_{1/2}(NPP) = 27$ h, $t_{1/2}(Hb) = 32$ h, and $s_{NPP} = s_{Hb} = 3$ h⁻¹. Open circles as in Fig 5. (B–D) Model-predicted, time-dependent changes in selected model variables relevant for the understanding of the mechanism behind the P_K/P_{Na} -generated different patterns, analyzed in detail in Discussion. Time-dependence is reported as a function of time post-invasion. Model simulations with (solid symbols) and without (open symbols) PK/PNa selectivity.

The model-derived explanation of the gentle and steep [Hb]-decline patterns when [Hb] is plotted as a function of the electron-probe-measured cNa/cK ratio (equal to the [Na]/[K] ratio) can be followed from the curves in Fig. 6 C. Comparison of the temporal courses of the [Hb] and [Na]/[K] curves shows that with no cation selectivity the [Hb] fall starts when the [Na]/[K] ratios are still very low, while [Hb] is increasing toward a peak value in the condition with $PK > PNa$. In this condition, [Hb] decline starts by the time Na-K gradient dissipation is already well advanced. Thus, when plotted as a function of the [Na]/[K] ratio, the [Hb]-decline patterns return the steep-gentle modalities observed.

The model analysis then allows for an interpretation of the observed [Hb]-decline patterns consistent with IRBC viability for both modalities. If the PK/PNa duality were real, how could it be explained?

One possibility, suggested to us by Dr. Serge L. Thomas (CNRS-UPMC, personal communication, 2010), is that the native cation selectivity ratio of NPPs is ~ 1 , and that the value of 2.3 obtained by Staines et al. (9) incorporates an additional PK component through activated IK1 channels (Gardos channels (42,43)), variably active in cultured IRBCs. An alternative possibility is that the Na-K selectivity of the NPP pathway can vary in cultures of the same *falciparum* strains initiated from different stabilates. Small variations in NPP-mediated cation selectivity can thus generate the marked differences in pattern of [Hb] decline documented here in Figs. 5 and 6 A. Further work will be needed to explore these possibilities.

The authors thank Lawrence Bannister and Serge Thomas for helpful discussions, and Evi Miklejewska, Janet Powell, and Toni Brain for instruc-

tions and maintenance related to the transmission electron microscopy, and for grid coating.

This work was supported by funds from the Engineering and Physical Sciences Research Council (grant No. EP/E059384) and the Biotechnology and Biological Sciences Research Council (grant No. BB/E008542/1). T.T. thanks the Isaac Newton Trust and the Wellcome Trust for support. A.E. was supported by the Engineering and Physical Sciences Research Council UK (grant No. EP/F044011/1).

REFERENCES

- Kirk, K. 2001. Membrane transport in the malaria-infected erythrocyte. *Physiol. Rev.* 81:495–537.
- Kanaani, J., and H. Ginsburg. 1988. Compartment analysis of ATP in malaria-infected erythrocytes. *Biochem. Int.* 17:451–459.
- Kanaani, J., and H. Ginsburg. 1989. Metabolic interconnection between the human malarial parasite *Plasmodium falciparum* and its host erythrocyte. Regulation of ATP levels by means of an adenylate translocator and adenylate kinase. *J. Biol. Chem.* 264:3194–3199.
- Bouyer, G., S. Egée, and S. L. Thomas. 2007. Toward a unifying model of malaria-induced channel activity. *Proc. Natl. Acad. Sci. USA.* 104:11044–11049.
- Ginsburg, H. 1988. How and why does the malarial parasite permeabilize its host cell membrane? In *Biomembranes: Basic & Medical Research*. G. H. Benga and J. M. Trager, editors. Springer-Verlag, Berlin, Germany. 188–203.
- Ginsburg, H., and W. D. Stein. 1987. New permeability pathways induced by the malarial parasite in the membrane of its host erythrocyte: potential routes for targeting of drugs into infected cells. *Biosci. Rep.* 7:455–463.
- Kanaani, J., and H. Ginsburg. 1991. Transport of lactate in *Plasmodium falciparum*-infected human erythrocytes. *J. Cell. Physiol.* 149: 469–476.
- Kirk, K., H. M. Staines, ..., K. J. Saliba. 1999. Transport properties of the host cell membrane. *Novartis Found. Symp.* 226:55–66, discussion 66–73.

9. Staines, H. M., A. Alkhalil, ..., S. A. Desai. 2007. Electrophysiological studies of malaria parasite-infected erythrocytes: current status. *Int. J. Parasitol.* 37:475–482.
10. Lee, P., Z. Ye, ..., R. G. Kirk. 1988. X-ray microanalysis of *Plasmodium falciparum* and infected red blood cells: effects of qinghaosu and chloroquine on potassium, sodium, and phosphorus composition. *Am. J. Trop. Med. Hyg.* 39:157–165.
11. Overman, R. R. 1947. Reversible permeability alterations in the erythrocytes of the malarious monkey. *Fed. Proc.* 6:174.
12. Staines, H. M., J. C. Ellory, and K. Kirk. 2001. Perturbation of the pump-leak balance for Na^+ and K^+ in malaria-infected erythrocytes. *Am. J. Physiol. Cell Physiol.* 280:C1576–C1587.
13. Ginsburg, H., S. Handeli, ..., M. Krugliak. 1986. Effects of red blood cell potassium and hypertonicity on the growth of *Plasmodium falciparum* in culture. *Z. Parasitenkd.* 72:185–199.
14. Dunn, M. J. 1969. Alterations of red blood cell sodium transport during malarial infection. *J. Clin. Invest.* 48:674–684.
15. Saliba, K. J., R. E. Martin, ..., K. Kirk. 2006. Sodium-dependent uptake of inorganic phosphate by the intracellular malaria parasite. *Nature.* 443:582–585.
16. Zarchin, S., M. Krugliak, and H. Ginsburg. 1986. Digestion of the host erythrocyte by malaria parasites is the primary target for quinoline-containing antimalarials. *Biochem. Pharmacol.* 35:2435–2442.
17. Krugliak, M., J. Zhang, and H. Ginsburg. 2002. Intraerythrocytic *Plasmodium falciparum* utilizes only a fraction of the amino acids derived from the digestion of host cell cytosol for the biosynthesis of its proteins. *Mol. Biochem. Parasitol.* 119:249–256.
18. Mauritz, J. M., A. Esposito, ..., V. L. Lew. 2009. The homeostasis of *Plasmodium falciparum*-infected red blood cells. *PLOS Comput. Biol.* 5:e1000339.
19. Lew, V. L., T. Tiffert, and H. Ginsburg. 2003. Excess hemoglobin digestion and the osmotic stability of *Plasmodium falciparum*-infected red blood cells. *Blood.* 101:4189–4194.
20. Lew, V. L., L. Macdonald, ..., T. Tiffert. 2004. Excess hemoglobin digestion by malaria parasites: a strategy to prevent premature host cell lysis. *Blood Cells Mol. Dis.* 32:353–359.
21. McConaghey, P. D., and M. Maizels. 1961. The osmotic coefficients of hemoglobin in red cells under varying conditions. *J. Physiol.* 155:28–45.
22. Adair, G. S. 1929. The thermodynamic analysis of the observed osmotic pressures of protein salts in solutions of finite concentration. *Proc. R. Soc. Lond.* 126:16–24.
23. Savitz, D., V. W. Sidel, and A. K. Solomon. 1964. Osmotic properties of human red cells. *J. Gen. Physiol.* 48:79–94.
24. Roberts, D. J., A. G. Craig, ..., C. I. Newbold. 1992. Rapid switching to multiple antigenic and adhesive phenotypes in malaria. *Nature.* 357:689–692.
25. Trager, W., and J. B. Jensen. 1976. Human malaria parasites in continuous culture. *Science.* 193:673–675.
26. Tiffert, T., H. M. Staines, ..., V. L. Lew. 2000. Functional state of the plasma membrane Ca^{2+} pump in *Plasmodium falciparum*-infected human red blood cells. *J. Physiol.* 525:125–134.
27. Pasvol, G., R. J. Wilson, ..., J. Brown. 1978. Separation of viable schizont-infected red cells of *Plasmodium falciparum* from human blood. *Ann. Trop. Med. Parasitol.* 72:87–88.
28. Jensen, J. B. 1978. Concentration from continuous culture of erythrocytes infected with trophozoites and schizonts of *Plasmodium falciparum*. *Am. J. Trop. Med. Hyg.* 27:1274–1276.
29. Cass, A., and M. Dalmark. 1973. Equilibrium dialysis of ions in nystatin-treated red cells. *Nat. New Biol.* 244:47–49.
30. Freedman, J. C., and J. F. Hoffman. 1979. Ionic and osmotic equilibria of human red blood cells treated with nystatin. *J. Gen. Physiol.* 74: 157–185.
31. Warley, A., and J. N. Skepper. 2000. Long freeze-drying times are not necessary during the preparation of thin sections for x-ray microanalysis. *J. Microsc.* 198:116–123.
32. Warley, A. 1997. X-Ray Microanalysis for Biologists. Portland Press, London and Miami.
33. Morgan, A., J. Brock, ..., G. Lewis. 1994. Mapping metal distributions in thin cryosections without scanning transmission electron microscope with the Phillips electron beam and image deflection (EBID) unit. *Scanning Microsc. Suppl.* 8:231–243.
34. Somlyo, A. V., G. McClellan, ..., A. P. Somlyo. 1985. Electron probe x-ray microanalysis of post-tetanic Ca^{2+} and Mg^{2+} movements across the sarcoplasmic reticulum in situ. *J. Biol. Chem.* 260:6801–6807.
35. Whitham, R. 1964. Transport and Diffusion in Red Blood Cells. Edward Arnold, London, UK.
36. Wunsch, S., C. P. Sanchez, ..., M. Lanzer. 1998. Differential stimulation of the Na^+/H^+ exchanger determines chloroquine uptake in *Plasmodium falciparum*. *J. Cell Biol.* 140:335–345.
37. Esposito, A., T. Tiffert, ..., V. L. Lew. 2008. FRET imaging of hemoglobin concentration in *Plasmodium falciparum*-infected red cells. *PLoS ONE.* 3:e3780.
38. Park, Y. K., M. Diez-Silva, ..., S. Suresh. 2008. Refractive index maps and membrane dynamics of human red blood cells parasitized by *Plasmodium falciparum*. *Proc. Natl. Acad. Sci. USA.* 105:13730–13735.
39. Lew, V. L., T. Tiffert, and H. Ginsburg. 2004. Response to: Allen and Kirk: cell volume control in the *Plasmodium*-infected erythrocyte. *Trends Parasitol.* 20:10–11.
40. Naughton, J. A., S. Nasizadeh, and A. Bell. 2010. Downstream effects of hemoglobinase inhibition in *Plasmodium falciparum*-infected erythrocytes. *Mol. Biochem. Parasitol.* 173:81–87.
41. Esposito, A., J. B. Choimet, ..., T. Tiffert. 2010. Quantitative imaging of human red blood cells infected with *Plasmodium falciparum*. *Biophys. J.* 99:953–960.
42. Gardos, G. 1958. The function of calcium in the potassium permeability of human erythrocytes. *Biochim. Biophys. Acta.* 30:653–654.
43. Vandorpe, D. H., B. E. Shmukler, ..., S. L. Alper. 1998. cDNA cloning and functional characterization of the mouse Ca^{2+} -gated K^+ channel, mIK1. Roles in regulatory volume decrease and erythroid differentiation. *J. Biol. Chem.* 273:21542–21553.